

Evaluating the Anti-Cancer Effect of Pomegranate Aqueous Extract of Gold Nanoparticles by Using Photodynamic Laser on Laboratory Mice.

Entidhar Jasim Khamees

Department of Physiology and medical physics, College of Medicine, University of Babylon

Email: intdher071@gmail.com, med.intidhar.jasim@uobabylon.edu.iq

<https://orcid.org/0000-0001-6149-5455>

Abstract

Background: This study evaluated the anticancer effects of gold nanoparticles (Au-NPs) generated by reducing hydrated gold metal ions in the presence of aqueous pomegranate peel extract.

Aim of study: To test the possibility that Au-NPs generated from the pomegranate aqueous extract could be employed as an anti-cancer therapy.

Materials and methods: The study aimed to evaluate Photodynamic therapy (PDT) using a laser at a wavelength of 532 nm with green gold particles as a photosensitizer in in-vivo experiment. Gold nanoparticles (Au-NPs) were produced by reducing hydrated gold metal ions in the presence of aqueous pomegranate peel extract. Using UV-visible spectroscopy, the absorption peak of the gold particles was found near 550-592 nm. All diffraction peaks for 2θ at = 37.8227° at 43.7014° , 63.8103° and 77.1540° correspond to the (111), (200), (220), and (311) levels, respectively by X-ray diffraction (XRD) analysis, imaging confirmed Au-NP by Transmission electron microscopy (TEM), the nanoparticle size ranged between 19.96 ± 0.784 nm. Forty Mature Swiss females weighing 20–25 g and aged 6–8 weeks were used, the animals were placed in well-ventilated rooms.

Results: The best exposure time to eradicate the tumor is with a duration of exposure of 30 minutes using the diode laser, as histological investigations indicated the development of anti-immunity with the same exposure period.

Keywords: Gold Nanoparticles, Pomegranate Aqueous Extract, Histopathological, Tumorbearing female mice.

Introduction

Nanotechnology is a field of science concerned with the investigation of materials in the nanoscale, which ranges from 1 to 100 nanometers. It is a nanoscale science that provides numerous focus points to many disciplines of research such as dentistry, pharmacology, and bioengineering⁽¹⁾. Scientific research on the manufacture of metal nanoparticles from natural sources such as plants⁽²⁾, fungus⁽³⁾, algae⁽⁴⁾, bacteria⁽⁵⁾, and viruses⁽⁶⁾ has expanded during this time. Because of their oxidation resistance, stability, and biocompatibility, Gold nanoparticles (Au-NPs) are among the most significant nanomaterials. Food packaging^(7,8), biomedical⁽⁹⁾, medication delivery, diagnostics, imaging⁽¹⁰⁾, and cosmetics can all benefit from Au-NPs⁽¹¹⁾. Several techniques have been tried for the green synthesis of gold NPs. Various quantities of Aloe vera (L) Burm. f. leaf extract were added to 6 mL of chloroauric acid (HAuCl₄) and distilled water was added to make the compound up to 10 mL. For Au-NP synthesis, the reaction mixture was permitted to stand for 30 hours⁽¹²⁾. A Musa acuminata Colla peel extract was pulverized and mixed with 1 mM of HAuCl₄ in a water bath for 3 minutes at 80°C to produce Au-NP (13). The pulp extract of Abelmoschus esculentus (L.) Moench was mixed with 1 mM of HAuCl₄ at a ratio of (4:1 v/v) for 6 hours at room temperature with continuous stirring. The solution was then kept undisturbed for further 18 hours⁽¹⁴⁾. 25 mL of 1 mM chloroauric acid (HAuCl₄) were added to mL of Zingiber officinale Roscoe root extract, and the solution was heated for 20 minutes⁽¹⁵⁾. According to the findings, MPPE43 Au-NPs are non-toxic, ecofriendly, and might be used as a biomaterial in

biomedical applications⁽¹⁶⁾. The use of the aqueous bark extract of Plumbago zeylanica for the production of Ag and Au-NPs is described⁽¹⁷⁾. The use of Pterocarpus santalinus L. (Red Sanders) bark extract to facilitate the fast stable environmentally friendly production of gold nanoparticles (Au-NPs)⁽¹⁸⁾. To produce nanoparticle, extracts of Quercus incana leaves were used to bioreduce tetrachloroauric acid (HAuCl₄-H₂O)⁽¹⁹⁾. At room temperature, Au-NPs were made to utilize a Solanum nigrum (S. Nigrum) leaf extract as a reducing agent⁽²⁰⁾. Current nanoparticle manufacturing processes are typically costly and include chemicals that may be detrimental to the environment, necessitating the creation of "greener" protocols. The synthesis of AuNPs by using plant extracts is described here; it provides an alternative efficient cheap and environmental friendly technique for producing well-defined nanoparticle geometries⁽²¹⁾. After several in vivo experiments, the present study suggests that Au-NPs generated from the pomegranate aqueous extract could be employed as an anti-cancer therapy.

Methods and Materials

Chemicals: A peel of the pomegranate was collected from the fruit. Then, the stock solutions of tetrachloroaurate salt (HAuCl₄) 99.98 percent) was obtained from Sigma as AuNPs. Distilled water was used to make the aqueous solutions and to clean and wash, all the glassware before use.

Preparing the Aqueous Pomegranate Peel Extract: The peels were first cleaned with tap water to remove dirt, rinsed with distilled water for several times, and then dried at 40°C in a laboratory oven. They were ground and turned into a fine extract out of which 0.50 g were added to 20 ml of distilled

water and boiled at 60 °C for 30 minutes. Then, the solution was cooled, filtered, put in a beaker, and kept for further use.

Synthesis of Au-NPs: At 25, 80, and 100°C°, 20 ml of peel extract was put into reaction with 10 milliliters of HAuCl₄ in a conical flask. Both the change in color and the time reaction took to change were noticed. The color of the solution almost instantly changes from pale brownish to red, indicating the creation of Au-NPs nanoparticles [Au/Pomegranate Pee] as shown in Figure (1) below.

The initial experiment (In-vivo experiment): The purpose of this study was to look into the effect of Photodynamic therapy (PDT) on mammary adenocarcinoma tumor growth inhibition.

Animal Model: Forty mature Swiss albino female mice weighing 20-25 grams and aged 6-8 weeks were used. At the College of Sciences/University of Babylon Animal Home, the animals were kept in well-ventilated chambers.

Transplantation of tumor cells in mice: A single tumor-bearing mouse (mammary adenocarcinoma) was provided from a prior experiment at the College of Veterinary Medicine/ University of Baghdad/ Cancer Unit. Tumor cells were collected for transplantation into mature female Swiss albino mice; the following procedure was used to carry out the transplanting process under extremely sterile circumstances 22:

- The tumor mass area was thoroughly cleaned with 70% ethanol.
- The contents of the tumor mass tissue were extracted using 10 ml disposable syringes, placed in a sterile flask, and

suspended in 50 ml of sterile PBS.

- 1 ml of tumor cell suspension was transplanted into an adult Swiss Albino mouse (4-6 weeks old) by inserting an 18-gauge needle hypodermic anywhere between the thigh and the shoulder.

Grouping the Experiment: The animals were divided into 10 groups, with four mice in each, as follows:

- **Group (G1)** is the negative control group for mice with no mammary adenocarcinoma.
- **Group (G2)** is the positive control group for mammary adenocarcinoma-bearing mice.
- **Group (G3)** is the PDT 25% AuNPs + laser group.
- **Group (G4)** is the PDT 12.6 % AuNPs + laser group.
- **Group (G5)** is the PDT 6.25 % AuNPs + laser group.
- **Group (G6)** for tumor-bearing mice injected with I/T 25 % AuNPs.
- **Group (G7)** for tumor-bearing mice injected with I/T 12.6% AuNPs.
- **Group (G8)** for tumor-bearing mice injected with I/T 6.25% AuNPs.
- **Group (G9)** for no mammary adenocarcinoma-bearing mice received AuNPs S/C injections.
- **Group (G10)** for tumor-bearing mice exclusively treated with laser.

Administration of Photosensitizer: Mammary adenocarcinoma cells (AM3) were subcutaneously implanted in the thigh area of female mice. After 2 weeks, the tumor has achieved the appropriate volume of at least 4.5 mm³.

Procedure for Laser Irradiation: Measuring and calculating the wavelength were carried out by using detectors manufactured in the

laboratory to find out the energy and its distribution on the laser beam, which appeared to be Gaussian. The laser power was then measured and the intensity was

extracted by using the relationship below:

$$I = P/\pi r^2 = 0.009 \text{ (W/cm}^2\text{)}^{(1)}$$

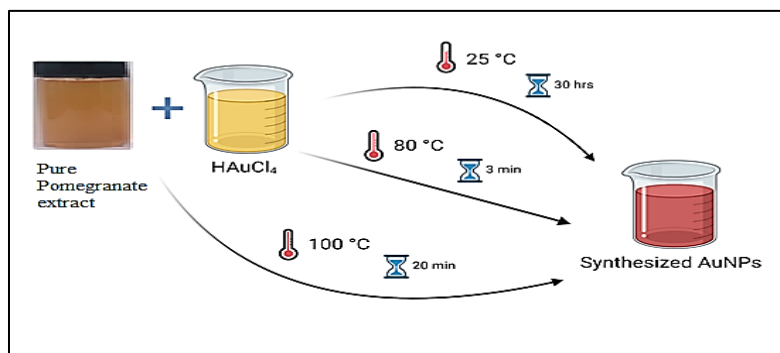


Figure 1: Green gold nanoparticle production methods (Au NPs).

Energy density (ED) is calculated from the relationship below:

$$(ED) = I t = 0.009 \times 30 = 0.27 \text{ Joule/cm}^2$$

where $I=0.009(\text{W/cm}^2)$ and the exposure time $t=30$ minutes.

Statistical analysis

The computations were performed by using the SPSS statistical software for social sciences (version 19) and Microsoft Office Excel (for examination of the specific significant differences among groups).

Results and Discussion

The pomegranate peel extract (0.50 g, 20 mL) acts as a reducing and stabilizing agent while HAuCl_4 (10 mM) acts as a gold precursor. The changes in the color of the extract has shown a reduction of HAuCl_4 , as shown in Figure (1).

The reaction was quick as the pale brownish color of the extracts turned red within 3 min,

20 min, and 30h, showing the formation of Au-NPs. The chemical equations for synthesizing the Au-NPs are as follows:



UV-Visible Spectroscopy Analysis: Figure (2) below shows UV-vis spectra that indicate the existence of Au-NPs. According to the findings, the pomegranate peel extracts have no discernible peak. However, when HAuCl_4 is added, a strong peak occurs near 593–532 nm. Other characterizations confirm that this signal implies the production of monodisperse spherical Au-NPs. Within 3min, 20min, and 30 h respectively, the reaction occurs with a noticeable color shift and (311) planes respectively; this indicates that Au-NPs have a face center cubic structure (fcc). By comparing the XRD pattern of Au-NPs to the

database, TCDD file number 96-901-2431 the crystallinity of Au-NPs is pure. However, there is a change in peaks with the database where pure metallic Au-NPs crystal structure is found. The Debye-Scherrer equation can be used to predict the particle size of Au-NPs.

$$d = \frac{k \lambda}{(\beta \cdot \cos \theta)} \quad (1)$$

where **d** denotes the average crystallite size, **k** the Scherrer constant (0.9), X-ray wavelength (0.154 nm), line broadening in radians, and θ is Bragg angle.

According to the Scherrer equation, the average crystallite size of Au-NPs is 13 nm.

Transmission Electron Microscopy (TEM):

The TEM was used to study the size and shape of the produced Au-NPs, as shown in Figure 4 below. The Au-NPs are well distributed with the pomegranate matrix around them showing that the pomegranate matrix functions as a capping agent to keep the Au-NPs from being aggregated. The produced Au-NPs have an average size of 19.96 ± 0.784 nm and are primarily spherical with occasional hexagonal and triangular shapes. *X-Ray Diffraction Analysis:* The crystalline structure of the Au-NPs produced is shown in Figure 3 below by the powder X-ray diffraction pattern. The spectra show a strong peak at $2\theta = 37.8227^\circ$, 43.7014° , 63.8103° , and 77.1540° which correspond to the (111), (200), (220),

Results of in vivo photodynamic therapy:

Clinical indicators include body weight, tumor volume, Tables (1,2).

A. Positive control group (G2)

The major clinical symptoms found in tumor-

bearing female mice were severe anorexia, resulting in gradual loss of body weight, accompanied by weakness, anemia, and cachexia, as shown in Table (1). All of these indications were observed with an increase in the tumor volume, in contrast with the negative control group (G1), as shown in Table (2) below.

B. Groups treated with PDT

In mice treated with PDT, the body weight increased within a normal range in groups (G3, G4 and G5), with no obvious clinical indications. However, the animals treated with Au-NPs showed a substantial drop in body weight only at the 3rd, 4th & 5th week of experiment in comparison with (G1).

C. Groups treated with Au-NPs

There was no significant difference in the body weight of tumor-bearing mice treated with different concentrations of Au-NPs at the first and second weeks, i.e., immediately after the intratumoral injection of Au-NPs. Yet, there was a significant difference in body weight during the last three weeks of the experiment. Table (1) shows that G6 and G7 have a similar significant difference.

D. Group treated with laser.

There was a significant decrease in the body weight of mice in G10, treated with laser only, in comparison with G1, at the last week of experiment.

The Effect of PDT on tumor volume

A. Positive control group (G2)

Indicating that the tumor was aggressive, the tumor volume increased in a time-dependent way in G2. However, the tumor volume and a high growth inhibition percent were reduced in the groups treated with PDT, as shown in Table (2). This is due to the effects of PDT.

B. Groups treated with PDT

As the results of tumor volume shown in Table (2), tumor volume was of significant inhibition rate at level of significance ($P < 0.05$). The tumor volume was decreased gradually during the five weeks of experiment reaching to (0.22 mm^3) in the (G3) treated with PDT (25% Au-NPs).

C. Groups treated with Au-NPs

Only the third week after I/T delivery of Au-NPs alone did tumor volume exhibit a significant drop at a level of significance ($P < 0.05$) in G6, G7, and G8. T+ 25, T+12.6, and T+ 6.25 percent of Au-NPs resulted in an increase in tumor volume to 7.06 , 7.58 , and 8.08 mm^3 respectively at the fifth week as shown in Table (2).

D. Groups treated with laser

Compared to G3, G4, and G5 treated diode laser (532nm) irradiation for 30 minutes without Au-NPs, Table (2) revealed a significant difference ($P < 0.05$). Besides, tumor volume grew significantly in G10, reaching 8.45 mm^3 at the fifth week of the experiment, compared to 8.58 mm^3 in G2 in the same week of the experiment.

Histopathological study:**A. Skin histopathology for G2.**

The microscopic findings G2 showed normal epidermis and dermis with skin appendages, as seen in the histological slice of skin in Fig. (5) below.

B. Microscopic lesion of breast adenocarcinoma tumor in G2. According to the histopathological findings, the malignant mass had infiltrated the subcutaneous tissue. It was made up of acinar-like structures, trabeculae, and islands of pleomorphic tumor cells with big hyperchromatic

nuclei and a proclivity to generate enormous cells, in addition to a great number of mitotic, as seen in Figure (6) below.

C. Skin PDT group G3 histopathology:

The results of a histological study of (G3), given a 25% dose, showed that the tumor mass was replaced by fibrous connective tissue infiltrated with inflammatory cells after AuNPs + laser irradiation. Meanwhile, the epidermis displayed thickening of the prickle cell layer (acanthosis) with widespread keratin deposition, as in figures (7, 8) below.

D. Skin histopathology for PDT groups G4 and G5.

The absence of the tumor mass was replaced by fibrous connective tissue infiltrated with inflammatory cells with significant fibrosis and edema development on histological examination of group (G4) treated with 12.6 percent of AuNPs + laser irradiation, as in Figure (9).

The histological results of the skin of tumor-bearing mice treated with PDT (6.25 percent AuNPs + laser irradiation) in G5 were comparable to those in G4, with mild fibrosis and clogged blood capillaries, as in Fig (10).

E. Skin histopathology in G6, G7, and G8 groups.

The skin of tumor-bearing mice in (G6, G7, and G8) treated simply with the photosensitizer AuNPs 25%, 12.61%, and 6.25% respectively showed comparable histological alterations, Figure (11), showing a remnant tumor mass buried in subcutaneous adipose tissue.

F. Histopathology of skin of group G9.

The major histological findings of skin in G9 tumor free mice injected with AuNPs 25% S/C include a significant sclerosis of the dermal layer with inflammatory cells

infiltration; hair follicles were dilated and infiltrated with dead neutrophils (Fig. 12,13).

G. Histopathology of skin of group G10.

The histology of skin tumor-bearing mice treated with laser alone (G10) revealed

comparable results to those in G2, with the tumor mass including subcutaneous tissue. It was made up of acinar-like structures, trabeculae, and islands of pleomorphic tumor cells with big hyperchromatic nuclei Figure (14).

Table 1: The Mean \pm SD of the PDT effect on the body weight (gm) of experimental groups during the five weeks of experiment.

Groups	1 st week	2 nd week	3 rd week	4 th week	5 th week
G1 Control -ve	19.67 \pm 1.08 A	19.6 \pm 1.08 A	20.1 \pm 1.10 a	21.11 \pm 1.15 a	22.2 \pm 1.08 a
G2 Control +ve	18.90 \pm 1.15 A	18.21 \pm 0.84 A	17.1 \pm 1.09 b	17.81 \pm 1.09 b	17.23 \pm 0.51 b
G3 PDT 25% AuNPs	19.1 \pm 2.08 A	19.78 \pm 1.71 A	20.1 \pm 1.68 a	21.01 \pm 1.68 a	22.50 \pm 1.41 a
G4 PDT 12.6 % AuNPs	18.7 \pm 3.10 A	19.68 \pm 2.91 A	20.08 \pm 2.37 a	21.08 \pm 2.37 a	22.6 \pm 2.96 a
G5 PDT 6.25 % AuNPs	18.17 \pm 1.32 A	19.6 \pm 1.32 A	20.6 \pm 1.32 a	20.6 \pm 1.32 a	20.25 \pm 2.25 a
G6 T+25% AuNPs	18.07 \pm 1.28 A	18.6 \pm 0.87 A	16.53 \pm 0.87 b	16.53 \pm 0.87 b	16.11 \pm 0.49 b
G7 T+ 12.6 % AuNPs	19.08 \pm 3.16 A	18.33 \pm 3.18 A	16.83 \pm 3.18 b	16.83 \pm 3.18 b	16.83 \pm 2.22 b
G8 T+ 6.25 % AuNPs	22.33 \pm 4.92 A	21.33 \pm 4.92 A	21.16 \pm 4.44 a	21.16 \pm 4.44 a	20.66 \pm 3.20 a
G9 S/C AuNPs	19 \pm 2.36 A	19.75 \pm 2.38 A	20.5 \pm 2.10 a	20.5 \pm 2.09 a	22.66 \pm 0.98 a
G10 T+L	18.67 \pm 2.60 A	18.63 \pm 2.02 A	18.05 \pm 1.15 a	18.05 \pm 1.15 a	16.83 \pm 0.98 a

Tukey's test revealed that the mean values of body weight (gm) followed by distinct letters differed substantially ($P < 0.05$) across experimental groups

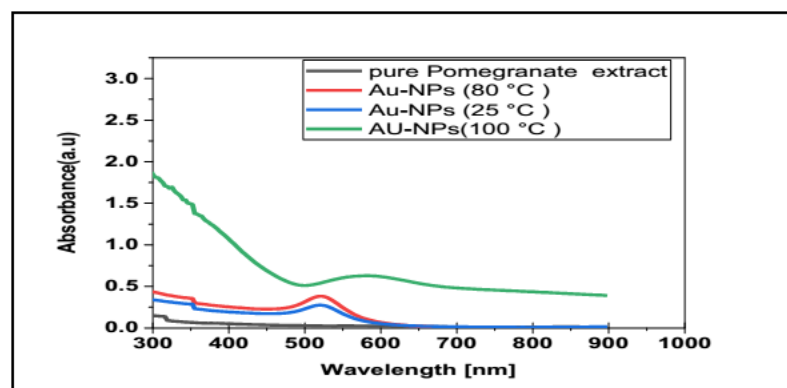


Figure 2: UV-Vis spectroscopy graph of synthesized Au-NPs. Pomegranate peel extracts.

Table 2: The Mean \pm SD of the tumor volume (mm^3) for the experimental groups during the course of the five-week trial.

Groups	0	1 st week	2 nd week	3 rd week	4 th week	5 th week
Control +ve	4.74 \pm 1.20 a	5.57 \pm 0.46 a	6.85 \pm 1.07 a	7.81 \pm 1.03 A	8.31 \pm 0.41 a	8.58 \pm 0.72 a
PDT 25% AuNPs	4.79 \pm 1.21 a	1.31 \pm 0.54 b	1.65 \pm 0.55 bc	1.39 \pm 0.52 bcd	0.87 \pm 0.77 b	0.22 \pm 0.58 bc
PDT 12.6 % AuNPs	4.79 \pm 0.18 a	2.23 \pm 0.21 b	3.12 \pm 0.68 b	2.37 \pm 0.63 bcd	1.85 \pm 0.37 bc	1.11 \pm 0.83 bc
PDT 6.25 % AuNPs	4.30 \pm 0.17 a	3.31 \pm 0.37 b	3.73 \pm 0.53 b	2.84 \pm 0.68 bc	2.43 \pm 0.36 bc	2.6 \pm 0.81 b
T+ 25% AuNPs	4.47 \pm 0.20 a	5.21 \pm 0.60 a	5.63 \pm 0.60 a	6.01 \pm 0.51 b	7.23 \pm 0.41 a	7.06 \pm 1.30 a
T+ 12.6 % AuNPs	4.23 \pm 0.28 A	4.85 \pm 0.50 a	5.53 \pm 1.05 a	5.88 \pm 0.91 b	7.10 \pm 0.56 a	7.58 \pm 0.94 a
T+6.25 % AuNPs	4.91 \pm 0.30 a	5.51 \pm 0.61 a	5.91 \pm 0.72 a	6.38 \pm 0.73 b	7.41 \pm 0.75 a	8.08 \pm 0.56 a
T+L	4.55 \pm 0.35 a	5.47 \pm 0.54 a	6.70 \pm 0.87 a	7.58 \pm 0.84 a	8.18 \pm 0.40 a	8.45 \pm 0.95 a

Tukey's test revealed that mean \pm .SD values followed by various tiny letters differed substantially ($P < 0.05$) across experimental groups.

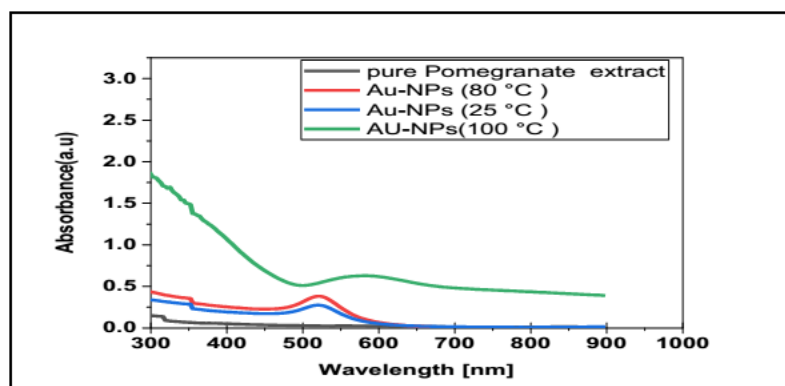


Figure 2: UV-Vis spectroscopy graph of synthesized Au-NPs. Pomegranate peel extracts.

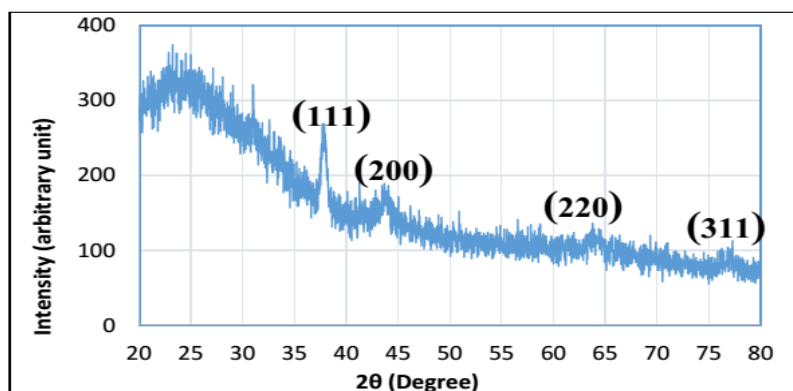


Figure 3: XRD spectra of Au-NPs prepared by pomegranate peel extracts with reference peak's intensity.

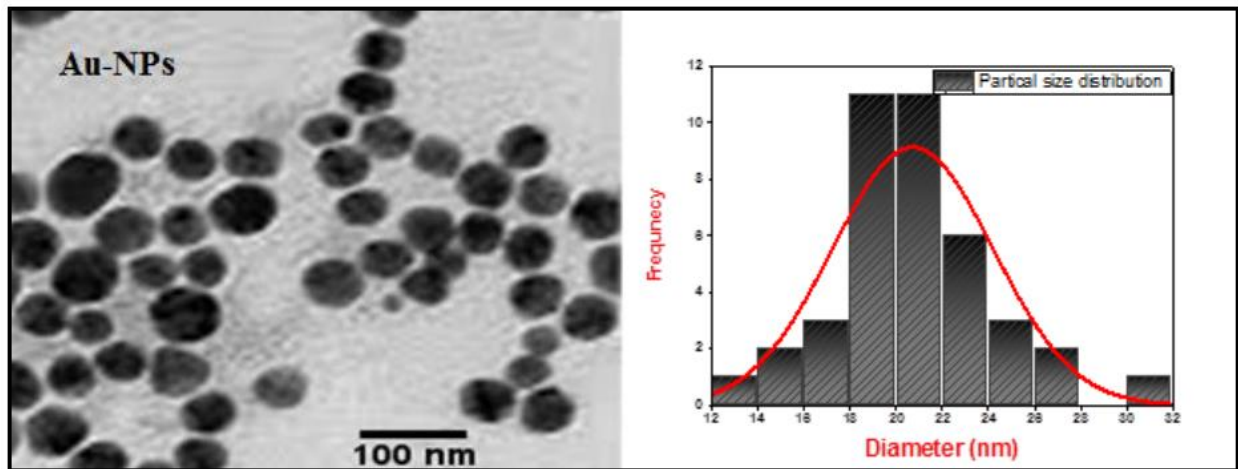


Figure 4: TEM image of Au-NPs formed by pomegranate peel extracts and the histogram of the particle size distribution of Au-NPs with $\times 250000$ magnification power.

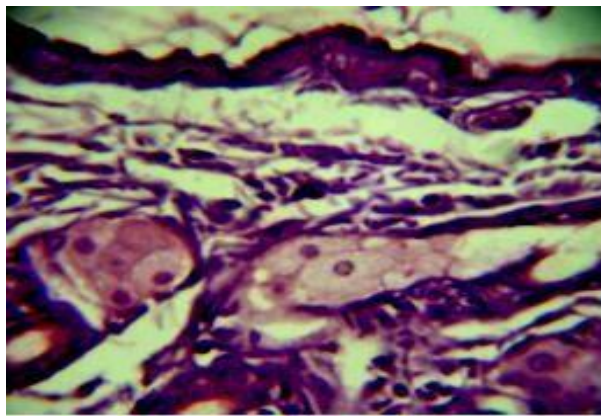


Figure 5: A Normal histological structure of mouse skin in a histological section, with power of magnification (400 X) control (-ve) group (G1).

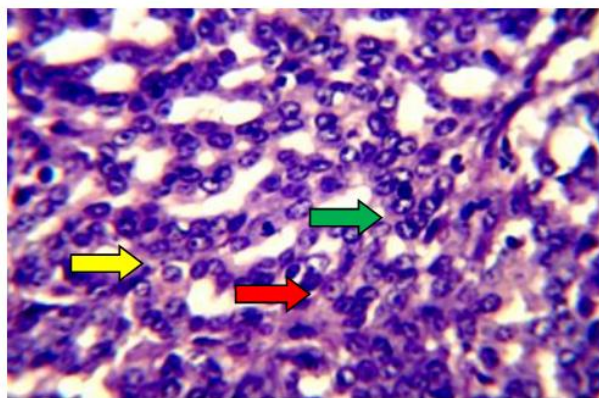


Figure 6: A histopathological section of a tumor mass in the skin of a tumor-bearing female mouse (control+ve group G2), demonstrating the growth of pleomorphic tumor cells () with hyperchromatic nuclei () & a large number of mitotic figures () (H&E stain with power of magnification 400x).

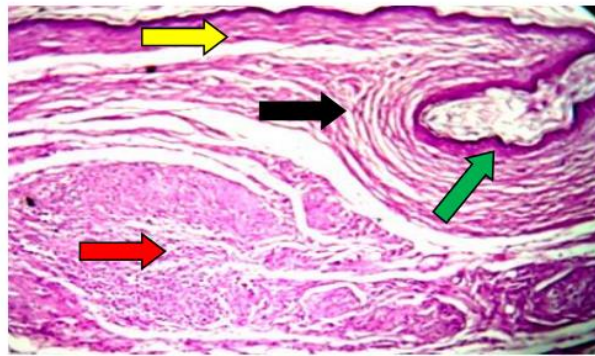


Figure 7: A histopathological segment of mouse skin (PDT group G3) exhibiting extensive fibrosis () with inflammatory cell infiltration () replacing the tumor mass with hyperkeratosis () & acanthosis () (H&E stain with power of magnification 100X).

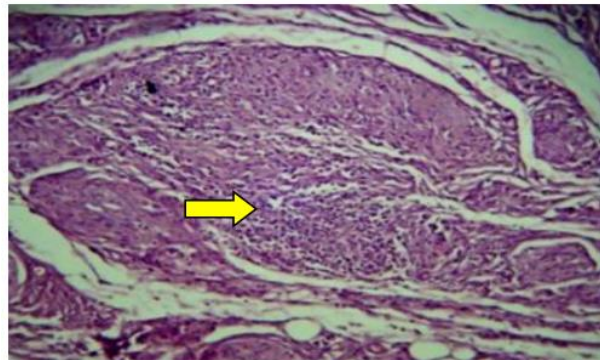


Figure 8: Fibrosis and inflammatory cells infiltration () replacing the tumor mass in a histopathological segment of mouse skin (PDT group G3) (H&E stain with power of magnification 400 X).

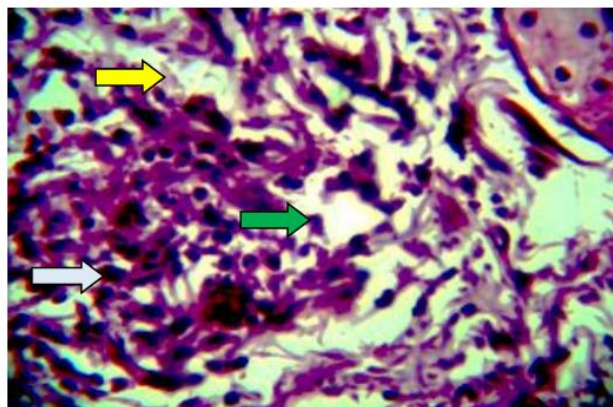


Figure 9: A Histopathological section of mouse skin in G11 demonstrating a moderate fibrosis () with inflammatory cell infiltration () and edema formation () (H&E stain with power of magnification 400 X).

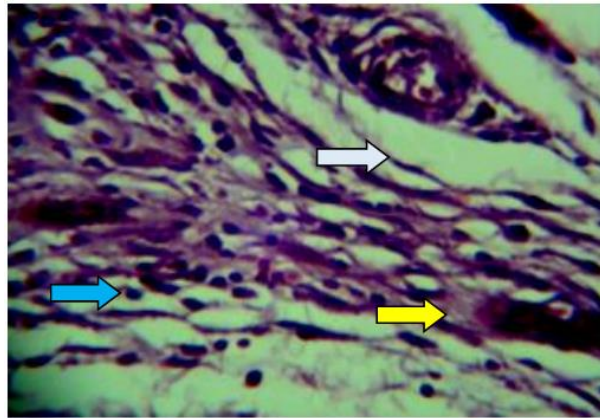


Figure 10: A Histopathological section of skin of G12 showing slight fibrosis () with few inflammatory cells infiltration () with congested blood capillaries () (H&E stain with power of magnification 400 X).

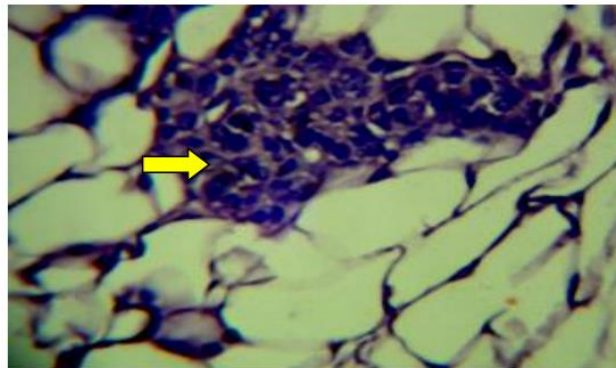


Figure 11: A histopathological section of tumor mass in the skin of tumor-bearing female mouse treated with 25% AuNPs only without laser (G6) showing remnant of tumor cells () within adipose tissue (H&E stain with power of magnification 400 X).

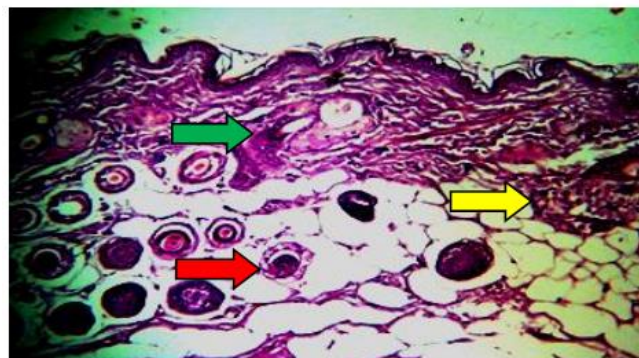


Figure 12: Sclerosis of the dermis () with inflammatory cell infiltration () with folliculitis () (H&E stain with power of magnification 100 X).

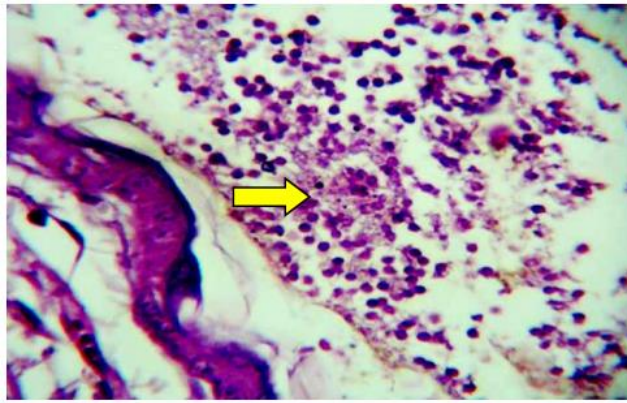


Figure 13: A histological section of mouse skin from G9 showing aggregations of large numbers of neutrophils on the surface () (H&E stain with power of magnification 400 X)

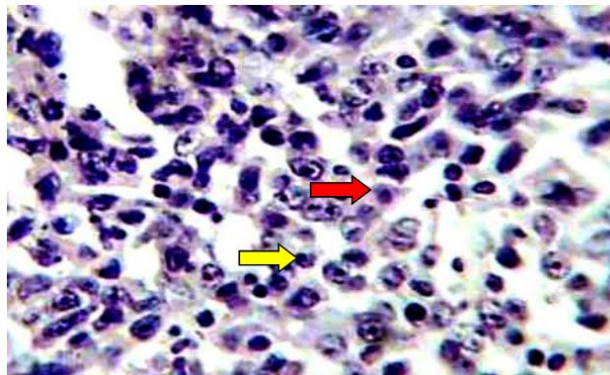


Figure 14: A histopathological section of tumor mass in skin of tumor-bearing female mouse in G10 showing the proliferation of pleomorphic tumor cells () with hyperchromatic nuclei () (H&E stain with power of magnification 400 X).

Conclusions

This study evaluated the anticancer effects of Au-NPs created by reducing aqueous gold metal ions in the presence of aqueous pomegranate peel extract. The study aimed to evaluate the photodynamic treatment using a laser with a wavelength of 532 nm with green gold particles as a photosensitizer in vivo experiments.

Increasing the exposure duration to 30 minutes by using a diode laser with an ED of 0.27 Joule/cm² after injecting 25% of Au-NPs intramurally resulted in a complete elimination of tumors in mammary adenocarcinoma-bearing mice. After

injecting 25% of Au-NPs into mammary adenocarcinoma-bearing mice, histological investigations indicated the development of anti-tumor immunity after 30 minutes of irradiation with a diode laser with an ED.

Biologically produced NPs can also be used in agriculture as an alternative to pesticides and herbicides, and to remove any hazardous microorganisms from water as well.

Acknowledgement

I would like to express my heartfelt gratitude to the College of Science, the University of Baghdad, and the Iraqi Center of Cancer and Medical Genetics for providing me with

laboratory mice. My gratitude extends to the staff of the Departments of Physics and Chemistry the College of Science, University of Babylon, and the Cancer Research Lab./ Wahj Al DNA).

Conflict of interest

The author states that she has no competing interests with respect to the publication.

References:

- Gour A and Jain N K. Advances in green synthesis of nanoparticles. *Artif. Cells, Nanomedicine Biotechnol.* 2019; 47(1): 844-851. doi:10.1080/2169140.2019.1577878.
- Rafi Shaik M, Qandeel Ali Z A, Khan M, Kuniyil M, Assal M E, Alkathlan H Z, *et al.* Green synthesis and characterization of palladium nanoparticles using origanum vulgare L. extract and their catalytic activity. *Molecules.* 2017; 22(1):1-12. doi: 10.3390/molecules22010165.
- Molnár Z, Bódai V, Szakacs G, Erdélyi B, and Fogarassy Z. Green synthesis of gold nanoparticles by thermophilic filamentous fungi. 2018; 8:1–12, doi: 10.1038/s41598-018-22112-3.
- González-Ballesteros N, Prado-López S, Rodríguez-González JB, Lastra M, & Rodríguez-Argüelles MC. Green synthesis of gold nanoparticles using brown algae *C. baccata*: I. activity in colon cancer *Cells* 2017;153:190-198. doi: 10.1016/j.colsurfb.2017.02/020.
- Javaid A and Oloketuyi SF. Diversity of Bacterial Synthesis of Silver Nanoparticles. doi: 10.1007/s12668-017-0496-x.
- Mohmed AA, Hassan SE, Fouda A, Elgamal MS, and Salem SS. Extracellular Biosynthesis of Silver Nanoparticles Using *Aspergillus* sp. and Evaluation of their Antibacterial and Cytotoxicity. 2017; 11(2):1–12. doi: 10.9734/JALSI/ 2017 /33491.
- Alnayli RS and Alkazaali H. Synthesis of silver nanoparticles by Nd:YAG laser and study Optical Limiting Behavior of colloid. *J. Kufa Phys.* 2019; 11(1): 7–12. doi: 10.31257/2018/ jkp/2019/ 110102.
- Paidari S and Ibrahim SA. Potential application of gold nanoparticles in food packaging: a mini review. *Gold Bull.* 2012; 54(1): 31–36. doi: 10.1007/s13404-021-00290-9.
- Elahi N, Kamali M, and Baghersad Talanta MH. Recent biomedical applications of gold nanoparticles: A review. *Talanta* 2018; 184: 537–556. doi: 10.1016/j.talanta. 2018.02.088.
- Kong FY, Zhang JW, Li RF, Wang Z X, Wang W J, & Wang W. Unique Roles of Gold Nanoparticles in Drug Delivery, Targeting and Imaging Applications. 2017; 22(9):1445. doi: 10.3390/molecules 22091445.
- Jiménez-pérez Z. E, Singh P, Kim Y J, Mathiyalagan R, Kim D H, Lee M H, *et al.* Applications of Panax ginseng leaves-mediated gold nanoparticles in cosmetics relation to antioxidant, moisture retention, and whitening effect on B16BL6 cells. *J. Ginseng Res* 2018; 42(3): 327–333. doi: 10.1016/j.jgr.2017.04.003.
- Mary V and Bert P. Synthesis of gold nanotriangles and silver nanoparticles using Aloe vera plant extract Related papers. 2006;22(2): 577-83. doi: 10.1021/bp0501423.
- Kumar AR. Banana peel extract mediated synthesis of gold nanoparticles Related papers. 2010; 80(1): 45-50. doi:10.1016/j.colsurfb.2010.05.029.
- Chakraborty M, Bhowmick B, Mondal D, Maity D, Rana D, Dash S K, *et al.* Anticancer (in vitro) and antimicrobial effect of gold nanoparticles synthesized using *Abelmoschus esculentus*. 2014; 4: 37838-37848 doi: 10.1039/c4ra07285e.
- Kumar A, Boruah BM, and Liang X. Gold Nanoparticles: Promising Nanomaterials for the Diagnosis of Cancer and HIV / AIDS. 2011, (2011): 22. doi: 10.1155/ 2011/202187).
- zeylanica bark Velammal P. antimicrobial and cytotoxic activities of silver and gold nanoparticles synthesized using, "Antioxidant, antimicrobial and cytotoxic activities of silver and gold nanoparticles synthesized using *Plumbago zeylanica* bark. *J. Nanostructure Chem* 2016; 6(3): 247–260, doi: 10.1007/s40097-016-0198-x.
- Sanders LR. Phytochemicals-mediated green synthesis of gold nanoparticles using *Pterocarpus santalinus* L. (Red Sanders) bark. 2017. doi: 10.1080/02726351.2017. 1302533.
- Sarwar R, Farooq U, Shah M R, Khan S, Riaz N, Naz S, *et al.* applied sciences Rapid Synthesis of Gold Nanoparticles from *Quercus incana* and Their Antimicrobial Potential against Human Pathogens. doi: 10.3390/app7010029.

- 19.** Gupta PK and Kim BS. Green Synthesis of Metallic Nanoparticles: Applications and Limitations. 2021, 1–35,
- 20.** Aljabali A, Akkam Y, Al Zoubi M A, Al-Batayneh K, Al-Trad B, Abo Alrob O, *et al.* Synthesis of Gold Nanoparticles Using Leaf Extract of *Ziziphus zizyphus* and their Antimicrobial Activity. *J. Nanomaterials* 2018; 8:1–15. doi: 10.3390/nano8030174